An OH Monitoring Method Using Infrared-Ultraviolet Double Resonance Laser-Induced Fluorescence

Kazuhide Tsuji, Kiyoshi Nakata, Hirotada Oishi, and Kazuhiko Shibuya*

Department of Chemistry, Graduate School of Science and Engineering, Tokyo Institute of Technology, 2-12-1 Ohokayama, Meguro-ku, Tokyo 152-8551

(Received July 5, 2000)

We have applied an infrared-ultraviolet double resonance laser-induced fluorescence (IR-UV LIF) technique to the measurement of OH concentrations in the troposphere. This OH exists in extremely low concentrations, ca. 10^6 molecules cm^{-3}, and plays a central role in the atmospheric chemistry. The detection limit of this new technique using our laser and detection system was experimentally determined to be 1.3×10^9 molecules cm^{-3} at 9.2 mTorr in Ar buffer gas. We have found that the method is free from chemical interferences but less sensitive than the single photon LIF method. A simple model is formulated and differential equations are numerically solved after the selection and determination of necessary physical constants. The method leads to the simulated (single photon LIF)/(IR-UV LIF) sensitivity ratio of 1.4×10^3, comparable with the experimental value of 2.2×10^3. On the basis of the proposed kinetic model, we discuss the optimum experimental parameters (sample pressure, IR and UV laser powers, and delay time) in this IR-UV LIF method by taking account of rotational energy transfer, fluorescence quenching, and saturation of absorption.

The HOx radical plays an important role in the atmospheric chemistry. As the chemical lifetime of OH is about one second due to its high reactivity with other atmospheric trace gases, the concentration of OH, [OH], is less than 1×10^7 molecules cm^{-3}, and depends strongly upon the ambient conditions, including the solar intensity in the ultraviolet region. Space- and time-resolved "*in situ*" measurements of [OH] are required to evaluate the chemical reaction model in the troposphere and to predict environmental changes in the near future. The technique is required to measure [OH] at the 1×10^5 molecules cm^{-3} level. The highly sensitive laser induced fluorescence (LIF) is one of the candidate methods suitable for detecting such a low concentration of OH. In the stratosphere, [OH] has been measured by LIF employing the $A^2\Sigma^+(v=1)\leftarrow X^2\Pi(v=0)$ excitation near 282 nm[1]. The collision-induced vibrational relaxation from $v=1$ to $v=0$ within the $A^2\Sigma^+$ state occurs, and the fluorescence intensity of the $A^2\Sigma^+(v=0)\rightarrow X^2\Pi(v=0)$ transition near 310 nm is measured. In the troposphere, there appeared severe problems in measurement of [OH] by the LIF method based on the same scheme as in the stratosphere[2]. The most serious problem arises from the artificial generation of OH by the laser light to monitor ambient OH. Ozone is photolyzed by ultraviolet light (< 320 nm) into $O(^1D)$ and O_2, and converted into artificial OH through the reaction of $O(^1D)$ with water. Rayleigh and Mie scattered light due to aerosols and fluorescence/chemiluminescence due to other trace gases also cause serious interference problems. Several groups have developed and improved the OH monitoring instruments using reduced-pressure LIF[3] originated in fluorescent assay by gas expansion (FAGE)[4], differential optical absorption spectrometry (DOAS)[5,6], and ion-assisted mass spectrometry[7]. The detection limits of these instruments are 4×10^4 cm^{-3} (reduced-pressure LIF, integration time = 5 min)[3], 1.5×10^6 cm^{-3} (DOAS, 6 min)[6], and 1×10^5 cm^{-3} (ion-assisted mass spectrometry, 5min)[7]. A special issue on such recent progress of the measurements of [OH] in the troposphere and stratosphere was reported in the *Journal of the Atmospheric Science*[8]. An intercomparison of DOAS[9] and LIF[10,11] methods was carried out during the field campaign POPCORN[12]. Results showed that both instruments measured [OH] reliably in clean air. Moreover, a model calculation study indicated that the laser-generated interference in the reduced-pressure LIF accounts for less than 1%[13].

As another methodology to overcome these interferences and to offer high selectivity and sensitivity, we have applied an infrared-ultraviolet double resonance laser-induced fluorescence (IR-UV LIF) technique to the measurement of OH concentrations in the troposphere. Bradshaw et al. originally proposed an IR-UV LIF method to measure [OH][14]. They reported a theoretical discussion of the detection limit in the troposphere. Schematic diagrams to excite and detect OH by single photon LIF and IR-UV LIF methods are shown in Fig. 1. In the single photon LIF, $A^2\Sigma^+(v=0$ or $1)\leftarrow X^2\Pi(v=0)$ transition is employed to excite OH, and the OH $A^2\Sigma^+(v=0)\rightarrow X^2\Pi(v=0)$ fluorescence is monitored. In the IR-UV LIF method, OH is first excited to the vibrationally excited state with the IR light through the $X^2\Pi(v=1)\leftarrow X^2\Pi(v=0)$ transition. Subsequently, OH $X^2\Pi(v=1)$ is further excited with the UV light near 350 nm to the electronically excited state through the $A^2\Sigma^+(v=0)\leftarrow X^2\Pi(v=1)$ transition. Then, the OH $A^2\Sigma^+(v=0)\rightarrow X^2\Pi(v=0)$ fluorescence at 310 nm is measured to determine [OH].

The advantages of IR-UV LIF will be summarized below.

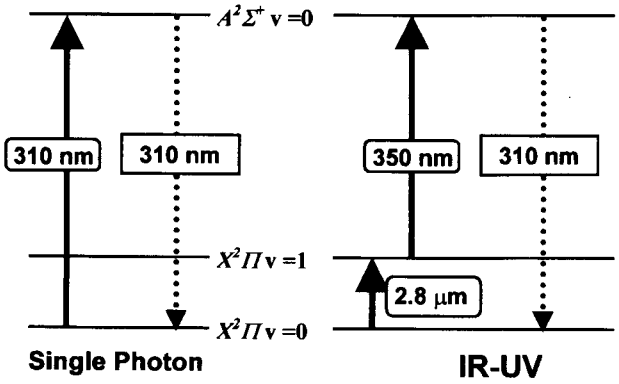

Fig. 1. Schematic transition diagrams to monitor OH employed in single photon LIF and IR-UV LIF methods.

(1) The UV laser used in the IR-UV LIF method is around 350 nm. The absorption cross section of ozone at 350 nm is much smaller than those at 310 nm or 280 nm, as listed in Table 1. The $O(^1D)$ quantum yields are not available for wavelengths longer than 335 nm and no $O(^1D)$ was detected in the photodissociation at 355 nm[17]. We therefore estimate that no $O(^1D)$ is generated by the photodissociation of ozone in the IR-UV LIF method, which results in no artificial OH generation. The chemical interference by ozone is, therefore, negligible in principle. (2) The fluorescence wavelength of 310 nm in the IR-UV LIF method is shorter than the UV laser light of 350 nm. Generally, excited molecules fluoresce in the wavelength region longer than that of the light absorbed. Therefore, the fluorescence of other trace gases covers the spectral region longer than the UV laser light. The light scattered by aerosol has the same wavelength as the UV laser light. Consequently, only the OH fluorescence light is located around 310 nm, while other fluorescence and scattered light sources are around 350 nm or even longer. Experimentally, it is rather easy to distinguish the OH fluorescence signal in the blue side from other signals in the red by using standard optical elements such as interference filters. (3) The above-mentioned advantageous features (1) and (2) of the IR-UV LIF method may allow us to monitor the ambient OH. The in situ measurement at the atmospheric pressure is important, because the low-pressure measurements using LIF and mass spectroscopy have inherent problems due to the OH losses on the sample inlet wall.

However, we must also mention some disadvantages of the IR-UV LIF method: (1) Two IR and UV laser systems are required and the instruments become complex. (2) The IR absorption bands of OH and water overlap each other in the same spectral region. The concentration of water is much higher than that of OH. The IR laser may be absorbed by ambient water and the effective IR laser power may be much reduced. In this work, we could avoid this optical interference by water, as mentioned later. (3) The detection sensitivity of the IR-UV LIF method might be lower than that of the single photon excitation LIF.

Table 1. Absorption Cross Sections and Quantum Yields for $O(^1D)$ Formation of O_3 at Three Wavelengths Corresponding to OH $A^2\Sigma^+ - X^2\Pi(0\text{–}1)$, (0–0), and (1–0) Transitions

$A^2\Sigma^+$–$X^2\Pi$ Transition		(0–1)	(0–0)	(1–0)
Wavelength/nm		346	310	284
σ_{O_3} [cm^2]	(Ref. 15)	6.41×10^{-22}	1.02×10^{-19}	2.712×10^{-18}
$\Phi_{O(^1D)}$	(Ref. 16)	$\cong 0$	0.60	0.92

In the present study, we characterized an IR-UV LIF method to measure [OH]. We determined the detection sensitivity of this method using the instruments in our laboratory, and compared it with that of a single-photon LIF method. Employing a master equation approach which took account of rotational energy transfer, fluorescence quenching, and saturation of absorption, we estimated the optimum experimental parameters (sample pressure, IR and UV laser powers, and delay time) in this IR-UV LIF method. It must be mentioned here that, in this study, we have not tried to design and construct our instruments for improving the sensitivity and reducing the background noise, because we are not concerned with the details of instruments at this moment.

Experimental

An overview of experimental setup and the flow chamber part employed for the IR-UV LIF method are shown in Figs. 2 and 3, respectively. The OH radical in a certain concentration was generated by a titration method using a reaction, $H+NO_2\rightarrow OH+NO$, under the conditions that a certain concentration of NO_2 was present with an excess concentration of H atom produced by a microwave discharge of H_2/Ar or H_2/He. We calculated [OH] using the flow rate of NO_2 and the pressure at the measurement zone. The flow chamber was pumped by a mechanical booster pump (ULVAC, PMB-001B) and a rotary pump (Alcatel, T2021C). The pressure was measured by using a capacitance manometer (MKS, Baratron 227HS-1). In order to obtain the correct pressure at the measurement zone, we compared the LIF intensity under flow conditions with that in the static cell containing a certain pressure of standard sample. We used

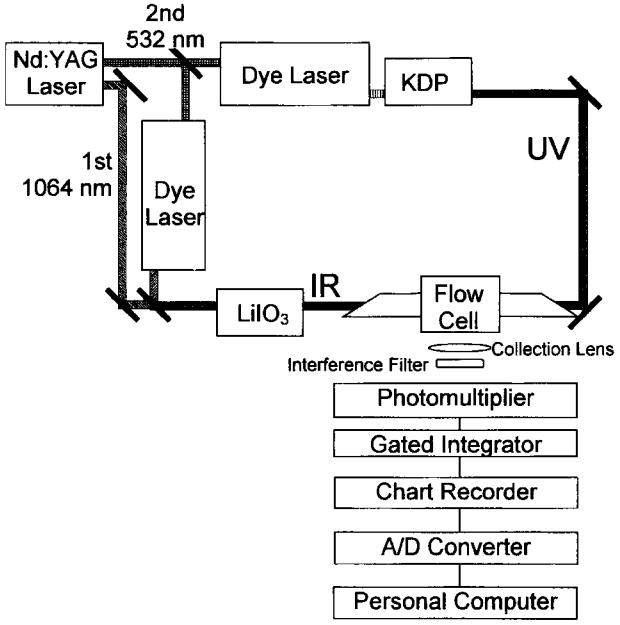

Fig. 2. Schematic view of experimental laser and detection setup.

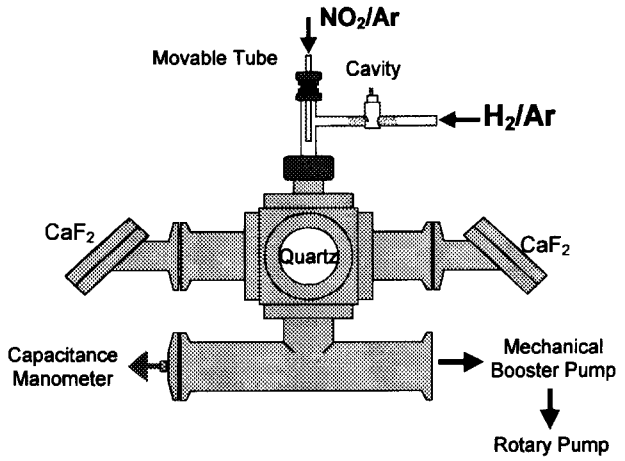

Fig. 3. Schematic view of flow cell.

NO gas as the standard sample, since its fluorescence quenching is negligibly small under the present experimental pressure conditions and its fluorescence quantum yield is almost unity. Typical flow rates of Ar, H_2, and NO_2 (1% diluted by Ar) were 1300, 27 and 4.2 $cm^3\ min^{-1}$, respectively, which resulted in the total pressure of 9.2 mTorr at the measuring zone (1 Torr $\approx$ 133.322 Pa). We employed this pressure condition because it was easy to control [OH] in our vacuum system.

The ν_{IR} light was generated in $LiIO_3$ (Inrad, IR-AutoTracker) by the difference-frequency mixing of 1.06 μm from the Nd : YAG laser (Lumonics HY750) and 770 nm from one dye laser (Lumonics HD300). The ν_{UV} light was generated by the frequency doubling of 700 nm from another dye laser using a KDP (potassium dihydrogenphosphate) crystal (Inrad, UV-Autotracker II). Both dye lasers were pumped by one Nd : YAG laser, which was also used as a 1.06 μm light source.

The OH fluorescence was collected by a quartz lens, selected by an interference filter (Corion, P10-310-F), and detected by a photomultiplier (Hamamatsu, 1P28). The output signal was averaged by a boxcar integrator (Stanford Research, SR-250), recorded by a chart recorder, and stored in a personal computer. The delay time between the first IR- and second UV-laser pulses was 5 ns.

The line selection of the IR transition is very important, since most IR absorption lines of OH and water overlap each other, as shown in Fig. 4. It is clear that the R and Q branches of OH are not suitable for the present purpose, and we employed the $P_1(4.5)$ line of OH $X^2\Pi(v = 1) - X^2\Pi(v = 0)$ transition at 3408 cm^{-1}, which is free from the overlapping problem.

In order to estimate the transition probability of OH $A^2\Sigma(v = 0) - X^2\Pi(v = 1)$, we measured the dispersed fluorescence (DF) spectrum using an imaging spectrograph (Chromex, 250IS) with a multichannel detector (Hamamatsu, C4563); this system is described elsewhere in detail[18]. We accumulated 10000 laser shots to obtain the accurate DF spectrum. The sensitivity of imaging spectrograph was calibrated by measuring the emission spectrum of a D_2-lamp as standard.

Results and Discussion

Figure 5 shows the IR-UV LIF excitation spectra of OH. The upper trace of Fig. 5a shows a ν_{UV}-scanned IR-UV LIF spectrum obtained by fixing ν_{IR} at 3407.53 cm^{-1} corresponding to the $P_1(4.5)$ line of $X^2\Pi(v = 1, J = 3.5) \leftarrow X^2\Pi(v = 0, J = 4.5)$. The two peaks at 28880.05 and 28880.82 cm^{-1} correspond to the doublet structure of OH $A^2\Sigma^+(v = 0, N = 3) \leftarrow X^2\Pi(v = 1, J = 3.5)$. The lower trace of Fig. 5a was obtained under exactly the same experimental conditions except that the IR laser was turned off. Only the background signal was recorded in the lower trace. It suggests that the concentration of vibrationally excited OH was

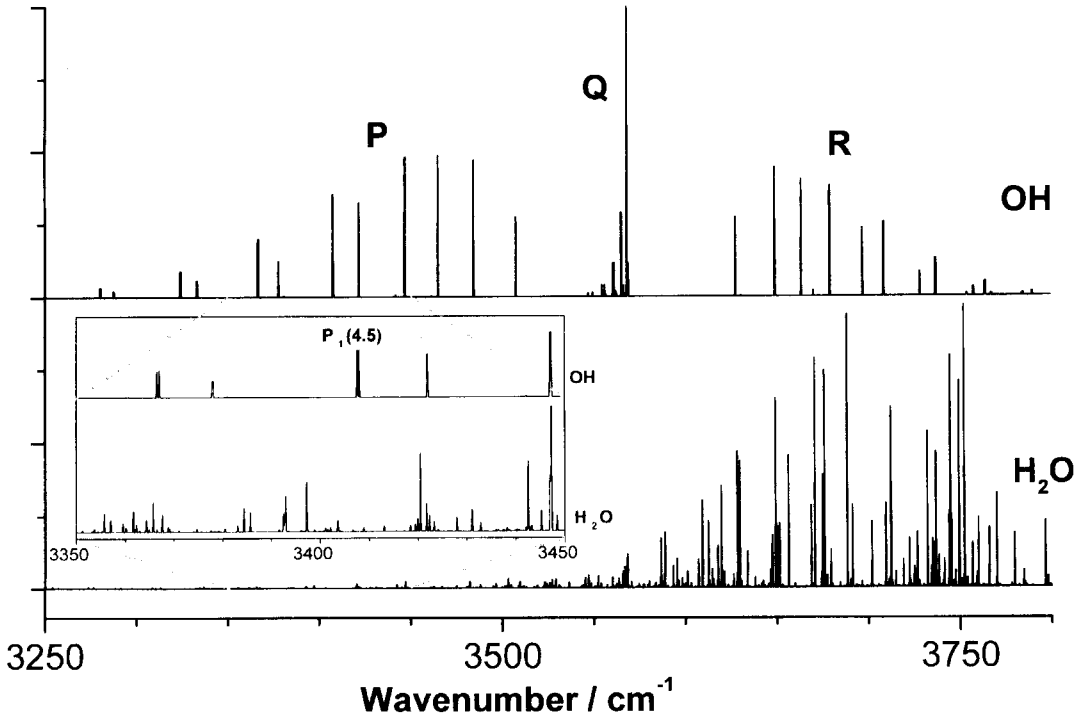

Fig. 4. IR absorption spectra based on HITRAN96 data base (http:www.hitran.com) of H_2O and OH. The line position of OH $P_1(4.5)$ employed in this IR-UV LIF method is indicated in the enlarged spectra (inset).

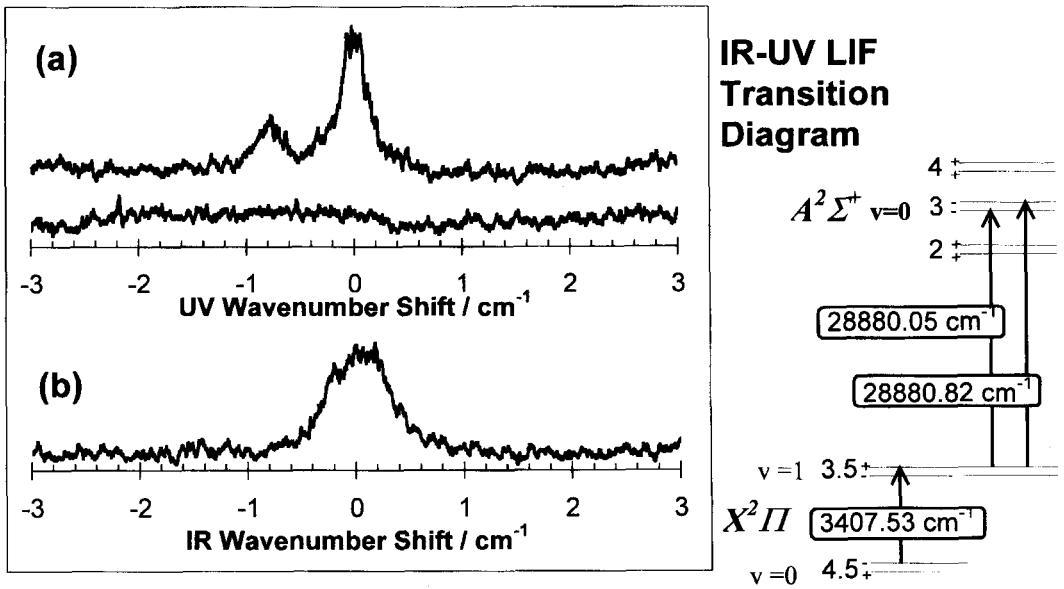

Fig. 5. IR-UV LIF excitation spectra of OH. These spectra were obtained under the pressure condition of 9.2 mTorr at the viewing zone. The zero shift wavenumbers are 28880.6 and 3407.5 cm^{-1} in the ν_{UV}- and ν_{IR}-scanned spectra, respectively.

negligibly low under the experimental conditions. We also measured the one photon LIF excitation spectrum of OH $A^2\Sigma^+(v = 0) \leftarrow X^2\Pi(v = 0)$, and estimated the rotational temperature of OH to be 300 K. These facts imply that the vibrationally- and rotationally-hot OH, produced by the reaction of NO_2 and H[19] was cooled down to room temperature before it reached the measuring zone of the fluorescence cell. Figure 5b shows a ν_{IR}-scanned IR-UV LIF spectrum, where ν_{UV} was fixed at 28880.8 cm^{-1} corresponding to the $Q_1(3.5)$ line of $A^2\Sigma^+(v = 0, N = 3) \leftarrow X^2\Pi(v = 1, J = 3.5)$. The ν_{IR} transition corresponds to a Λ doublet component of $P_1(4.5)$ line of OH $X^2\Pi(v = 1, J = 3.5) \leftarrow X^2\Pi(v = 0, J = 4.5)$. The overall transition diagram is also shown in Fig. 5. The linewidths measured in Fig. 5 correspond to the spectral resolutions of the lasers. We, thus, succeeded to detect OH in the concentration around 10^{10} molecules cm^{-3} using the IR-UV LIF method. We could not observe any rotational line originating with the rotational levels of $J \neq 3.5$ in the $A^2\Sigma^+(v = 0) \leftarrow X^2\Pi(v = 1)$ transition, when ν_{IR} was fixed at 3408 cm^{-1}. The rotational energy transfer within $X^2\Pi(v = 1)$ was negligible under the present experimental conditions.

The IR-UV LIF intensity linearly depends on the radical concentration, [OH], as shown in Fig. 6. The concentration of OH was controlled by adjusting the flow rate of the NO_2/Ar gas mixture. The IR and UV laser powers were 100 μJ and 10 μJ, respectively. From the linear relationship between IR-UV LIF intensity and [OH], the detection sensitivity of this technique is determined as the OH fluorescence intensity divided by the OH concentration. The detection sensitivity of single photon LIF in the $A^2\Sigma^+(v = 0) \leftarrow X^2\Pi(v = 0)$ transition is also determined from the independent experimental results using the same experimental setup with the UV laser power of 10 μJ. The ratio of the detection sensitivity of the single photon LIF method to that of the IR-UV LIF method is evaluated to be 2.2×10^3.

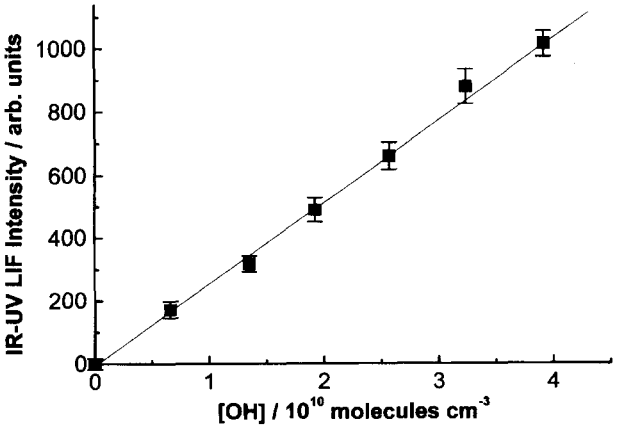

Fig. 6. Calibration curve of OH in IR-UV LIF method.

We calculate the detection sensitivity ratio to compare it with the experimental value of 2.2×10^3. The total pressures around 10 mTorr employed in our experiment were low enough to allow us to neglect the quenching of OH $A^2\Sigma^+$. The density of OH $A^2\Sigma^+$ generated by the IR-UV LIF method is estimated by solving the following sequential differential equations (1) and (2), which describe spontaneous and induced processes among the ground state ($X^2\Pi$, $v = 0$), the vibrationally-excited state ($X^2\Pi$, $v = 1$), and the electronically-excited state ($A^2\Sigma^+$, $v = 0$). In the present calculation, we neglect the UV emission processes to the vibrational excited levels ($v \geqq 1$) because of small Franck–Condon factors[20].

$$\frac{dN_3}{dt} = B_{23}\overline{W}_{23}(t)N_2 - B_{32}\overline{W}_{23}(t)N_3 - A_{31}N_3 \quad (1)$$

$$\frac{dN_2}{dt} = B_{12}\overline{W}_{12}(t)N_1 - B_{21}\overline{W}_{12}(t)N_2 + B_{32}\overline{W}_{23}(t)N_3 - B_{23}\overline{W}_{23}N_2 \quad (2)$$

$$N_1 + N_2 + N_3 = N_{total} \quad (3)$$

Here, the subscript numbers "1", "2", and "3" denote $X^2\Pi(v = 0)$, $X^2\Pi(v = 1)$, and $A^2\Sigma^+(v = 0)$, respectively.

N_1, N_2, and N_3 are the time-dependent densities of OH in $X^2\Pi(v=0)$, $X^2\Pi(v=1)$, and $A^2\Sigma^+(v=0)$, respectively. N_{total} is the total density of OH. Symbols B_{ij}, A_{ij}, and $\overline{W}_{ij}(t)$ are the Einstein B coefficient, Einstein A coefficient, and the time evolution of the laser photon flux, respectively. In the single photon LIF method, we need to solve a sequential differential equation:

$$\frac{dN_3}{dt} = B_{13}\overline{W}_{13}(t)N_1 - B_{31}\overline{W}_{13}(t)N_3 - A_{31}N_3 \quad (4)$$

$$N_1 + N_3 = N_{\text{total}} \quad (5)$$

In order to estimate the transition probability A_{32} for the $A^2\Sigma^+(v=0)-X^2\Pi(v=1)$ band, we measured the DF spectrum via the $A^2\Sigma^+(v=0)$ state, as shown in Fig. 7. From the intensity ratio between the $A^2\Sigma^+(v=0)\rightarrow X^2\Pi(v=0)$ and the $A^2\Sigma^+(v=0)\rightarrow X^2\Pi(v=1)$ emission bands, the transition probability ratio A_{31}/A_{32} is estimated to be $(4.4\pm0.4)\times10^{-3}$. Our value agrees well with the value of 4.8×10^{-3} calculated by using RKR potentials[20] and is a bit larger than the experimental value of $(3.7\pm0.8)\times10^{-3}$ [21]. Einstein A coefficients used in the Eqs. 1, 2, 3, 4, and 5 are listed in Table 2; the corresponding B coefficients have been derived by using the A coefficients. The Eqs. 1, 2, 3, 4, and 5 have been solved on the assumption that the time evolution of the laser pulse, $\overline{W}(t)$, is described as a Gaussian function with 8 ns pulse width. The relative detection sensitivity is evaluated as the ratio of the density of OH in the A state after the UV laser pulse excitation in the single photon LIF method to that in the IR-UV LIF method. The simulated detection sensitivity ratio is obtained to be 1.4×10^3, which is almost two times smaller than the experimental value of 2.2×10^3. We believe both values agree reasonably with each other, considering the lack of uniformity in spatial flux distribution of the laser beams and the incomplete spatial overlapping of two laser beams.

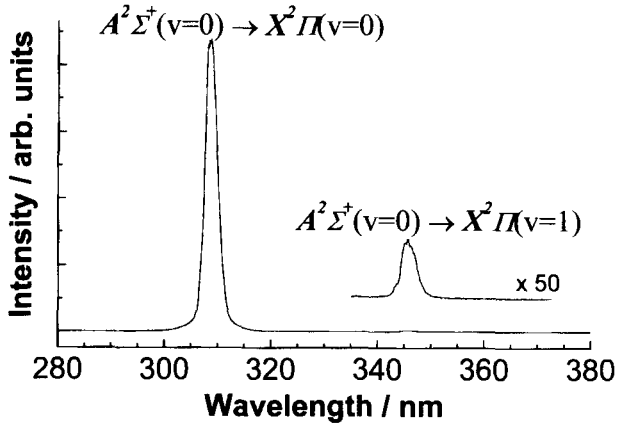

Fig. 7. Dispersed fluorescence spectrum of OH via the $A^2\Sigma^+(v=0)$ state.

From the analysis of the calibration line shown in Fig. 6, we can determine the detection limit of our IR-UV instrument, which is defined as the minimum detectable concentration corresponding to the signal-to-noise (S/N) ratio of 2. The detection limit of the IR-UV LIF method using our laser and fluorescence detection systems is thus estimated to be 1.3×10^9 molecules cm^{-3} at 9.2 mTorr in Ar buffer gas with an integration time of 10 s. The poor detection limit was controlled mainly by intense background noise due to the scattered light of probe UV laser light. Our instruments were designed to detect IR-UV LIF signals, but no efforts for reducing the scattered light were made in the present study because our purpose is to characterize the various parameters important in the IR-UV LIF method. The noise level will be much lowered by improving the fluorescence collecting optics, such as a fluorescence cell, interference filters, lenses, and so on. The low repetition frequency of the laser and the short integration time are other reasons for the poor detection limit. Measurements using a laser system with higher repetition frequency and employing a longer integration time make the S/N ratio higher and improve the detection limit accordingly.

In general, the detection limit is governed by many experimental parameters and conditions, such as laser power, sample pressure, optical design, photo-detector and so on. For example, if we perform the IR-UV LIF experiment under the conditions of atmospheric pressure, it is necessary to consider the influence of the collision-induced rotational energy transfer in the intermediate vibrationally-excited state ($X^2\Pi$, $v=1$) and the initial ground state ($X^2\Pi$, $v=0$), and the fluorescence quenching of the electronically-excited state ($A^2\Sigma^+$, $v=0$). In the following discussion, we optimize the experimental parameters (IR and UV laser powers, sample pressure, and IR-UV delay time) in the IR-UV LIF method by taking account of rotational energy transfer, fluorescence quenching, and saturation effect of absorption processes. The vibrational relaxation process is neglected since the rate constant is less than 10^{-14} cm^3 $molecule^{-1}$ s^{-1} [24]. The quenching rate constants of OH $A^2\Sigma^+$ ($v=0$) by N_2 and O_2 are 0.19×10^{-10} and 1.25×10^{-10} cm^3 $molecule^{-1}$ s^{-1}, respectively[25], which leads to the estimation of the quenching constant for dry air to be 0.4×10^{-10} cm^3 $molecule^{-1}$ s^{-1}. Under the atmospheric pressure conditions, OH radicals in the $A^2\Sigma^+$ state are actually quenched and only 0.15% emit fluorescence. Concerning the rotational energy transfer, we employ an ex-

Table 2. Einstein A Coefficients and the Laser Bandwidths Used in This Work

Transition	Einstein A Coefficient / s^{-1}		Laser Bandwidth / FWHM/cm^{-1}
$A^2\Sigma^+(v=0)$–$X^2\Pi(v=0)$ $P_1(4.5)$	4.567×10^5	(Ref. 22)	0.3
$A^2\Sigma^+(v=0)$–$X^2\Pi(v=1)$ $Q_1(3.5)$	2.5×10^3	(this work)	0.3
$X^2\Pi(v=1)$–$X^2\Pi(v=0)$ $P_1(4.5)$	14.176	(Ref. 23)	0.8

ponential-gap model proposed by Kliner and Farrow[26] for the state-to-state rotational energy transfer. A master equation is used to calculate the IR-UV LIF intensities under the various conditions, taking account of the optical and physical processes shown in Fig. 8.

Figure 9 shows the calculated IR-UV LIF intensity under various conditions. In the simulation, the IR and UV laser powers employed are 100 μJ and 10 μJ, respectively, which are the same as those in our experiments. The IR-UV LIF intensity is normalized to the value calculated by using the pressure condition (9.2 mTorr) we employed in our experiments. With increasing the pressure, the IR-UV LIF intensity rises to the peak and gradually decreases, as shown in Fig. 9a. The rise of the IR-UV LIF intensity in a lower pressure region is due to the increasing OH concentration. The decrease in a higher pressure region is caused by the collisional processes due to the ambient gases: the rotational energy transfer of the intermediate state ($X^2\Pi$, $v = 1$) and the quenching of the electronically-excited state ($A^2\Sigma^+$, $v = 0$). The maximum intensity is obtained at the sample pressure of 4.7 Torr and is 78 times stronger than the IR-UV LIF intensity at 9.2 mTorr. Figures 9b and 9c show how the IR-UV LIF intensity depends on the delay time between the two laser pulses. Under the sample pressure of 760 Torr shown in Fig. 9b, the relative intensity rises with the delay time and the intensity is steady at 32. This delay time profile is due to the fast rotational energy transfer in OH $X^2\Pi(v = 1)$. Under the sample pressure of 4.7 Torr shown in Fig. 9c, the relative intensity rises with the delay time and the maximum intensity of 81 is obtained at the delay time of 7 ns. The excitation process due to the UV laser pulse competes with the rotational energy transfer. We have shown that the detection limit is improved by changing the experimental conditions of sample pressure and delay time, although the laser powers are kept constant.

Figures 10a and 10b show the laser power dependence of the relative IR-UV LIF intensities under the sample pressures of (a) 760 Torr and (b) 4.7 Torr, respectively. The solid lines represent the relative IR-UV LIF intensity, which is also normalized to the value calculated based on the pressure (9.2 mTorr) and laser power (IR = 100 μJ and UV = 10 μJ) conditions we employed in our experiments. The intervals of contour lines of the relative IR-UV LIF intensities become wider as the IR or UV laser power increases. The relative intensities are not proportional to the IR and UV laser powers, due to the so-called saturation effect of absorption. The saturation of absorption at 760 Torr is less effective due to the very fast rotational energy transfer in the intermediate $X^2\Pi(v = 1)$ state and the efficient quenching process of the excited $A^2\Sigma^+(v = 0)$ state. The saturation parameter (S) is derived using a relation, $S = (\alpha_0/\alpha)\text{-}1$, where α and α_0 are the saturated and unsaturated absorption coefficients, respectively[27]. The relative absorption coefficient α for the present double resonance process is calculated by dividing the IR-UV LIF intensity by the IR and UV laser powers. The unsaturated absorption coefficient of α_0 is calculated under the minimum IR and UV laser power conditions. The bro-

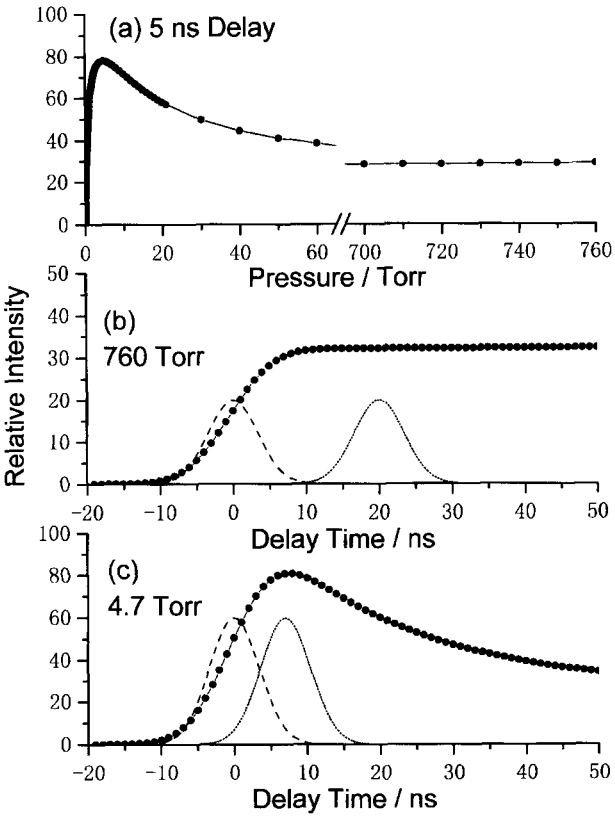

Fig. 9. Relative IR-UV LIF intensities calculated under various conditions. The IR and UV laser powers are fixed at 100 μJ and 10 μJ, respectively. The intensities are normalized to the IR-UV LIF intensity at 9.2 mTorr. (a) Sample pressure dependence of relative IR-UV LIF intensity. The delay time between IR and UV laser pulses is fixed at the experimental value (5ns). (b) Delay time dependence of relative IR-UV LIF intensity. The sample pressure is fixed at 760 Torr. The broken and dotted lines represent the time profiles of the IR (0 ns) and UV (20 ns) laser pulses, respectively. (c) Delay time dependence of relative IR-UV LIF intensity. The sample pressure is fixed at 4.7 Torr. The broken and dotted lines represent the time profiles of the IR (0 ns) and UV (7 ns) laser pulses, respectively.

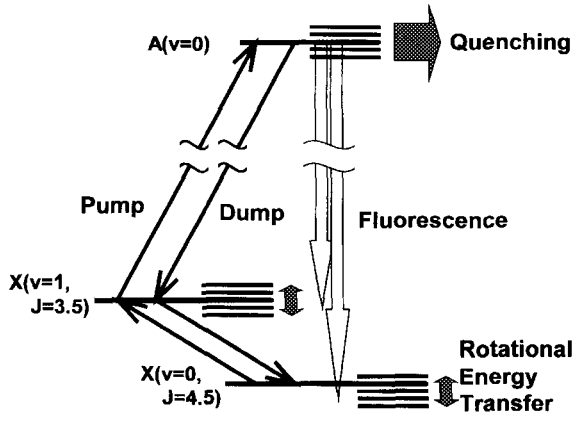

Fig. 8. Kinetic model employed in our simulation of IR-UV LIF intensity to optimize the experimental conditions.

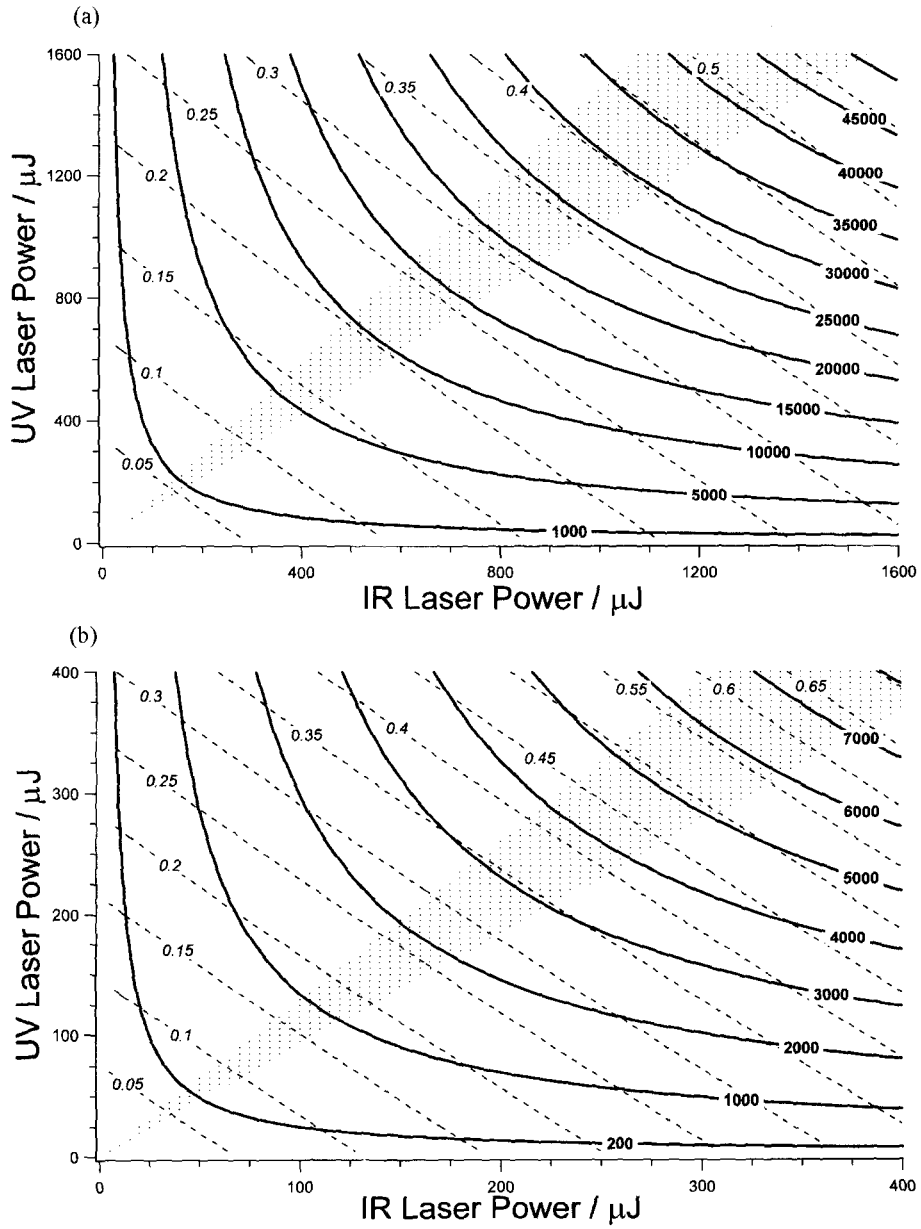

Fig. 10. Laser power dependence of IR-UV LIF intensity. Solid and broken contour lines represent the relative IR-UV LIF intensities (200—50000) and saturation parameters (0.05—0.70), respectively. The intensities are normalized to the IR-UV LIF intensity at 9.2 mTorr. (a) Sample pressure = 760 Torr and IR-UV delay time = 20 ns and (b) 4.7 Torr and 7 ns.

ken lines in Fig. 10 represent the saturation parameter (S). Considering the saturation parameters, we conclude that the sample pressure of 760 Torr is suitable for the IR-UV LIF measurement, since in the near future we will be able to use much more powerful lasers and the detection limit will be much improved. Let us carry out a sample IR-UV LIF experiment under the saturation parameter of 0.1. The relative intensity of 2823 is obtained by a 280 μJ IR laser and a 340 μJ UV laser at 760 Torr, while only the intensity of 386 is obtained by a 65 μJ IR laser and a 75 μJ UV laser at 4.7 Torr. This clearly indicates that one of the great advantages in the IR-UV LIF method is that it can be applied to the atmospheric-pressure measurements and the detection limit in the IR-UV LIF method is much improved in the atmospheric-pressure measurements. Figure 10 shows that various sets of IR and UV laser powers give a certain IR-UV LIF intensity with different saturation parameters. The smaller laser power is better for the quantitative measurements in general. One can derive the ideal relation between the IR and UV laser powers from Fig. 10; [UV laser power] $\approx 1.2\times$[IR laser power] at 760 Torr and [UV laser power] $\approx 1.1\times$[IR laser power] at 4.7 Torr.

The IR-UV measurement might be carried out under the extreme conditions in which the IR absorption is completely saturated and the OH population in the $X^2\Pi(v=1)$ state is almost the same as that in the $X^2\Pi(v=0)$ state. The possibility of IR multiphoton absorption is considered. Fortunately, the absorption line ($P_1(4.5)$ line of $X^2\Pi(v=1)\leftarrow X^2\Pi(v=0)$) employed in the present experiment does not overlap with any absorption line in the $X^2\Pi(v=2)\leftarrow X^2\Pi(v=1)$ tran-

sition. The absorption line nearest to the $P_1(4.5)$ line of $X^2\Pi(v=1)\leftarrow X^2\Pi(v=0)$ is the $Q_2(0.5)$ line of $X^2\Pi(v=2)\leftarrow X^2\Pi(v=1)$ at 3403.6 cm^{-1}, which is 4 cm^{-1} apart from the $P_1(4.5)$ line of $X^2\Pi(v=1)\leftarrow X^2\Pi(v=0)$. Thus the possibility of the IR multiphoton absorption is safely excluded. Such saturation conditions in the IR absorption at 760 Torr will be realized by using a powerful 10 ns-pulsed IR laser with a pulse energy of about 20 mJ. Another way to reach the saturation conditions is to use a cw-IR laser and a Fabry–Perot resonator[28]. Under these saturation conditions, the IR-UV LIF method is regarded as a simple one-photon LIF method to monitor OH $X^2\Pi(v=1)$, the concentration of which is nearly the same as that of OH $X^2\Pi(v=0)$. This method has something in common with the 282 nm excitation LIF method proposed in the early 1970's[2]. In the 282 nm excitation LIF method, OH was excited to $A^2\Sigma^+(v=1)$ and relaxed to the $A^2\Sigma^+(v=0)$ by the collision with ambient gases. The fluorescence band detected near 310 nm was due to $A^2\Sigma^+(v=0)\rightarrow X^2\Pi(v=0)$, which was 30 nm red-shifted from the excitation laser line. This method seemed to be adequate for measuring [OH] at atmospheric pressure in the troposphere, except for the serious interference problem due to the artificial OH generation[2]. Both in the present IR-UV LIF method and in the 282 nm excitation LIF method, the OH fluorescence is detected at 310 nm, which shifts largely from the excitation wavelengths (350 and 282 nm, respectively). Both methods can be employed under atmospheric pressure conditions. In the present method, [OH] can be measured with the 346 nm laser, the power of which is roughly estimated to be 150 ($= 2A_{10}/A_{01}$[20]) times as intense as that in the 282 nm excitation LIF method.

In conclusion, the IR-UV LIF method is found to be all-purpose, highly sensitive, and free from chemical interferences in combination with a powerful laser system. Although our goal to measure atmospheric OH concentrations by using the IR-UV LIF method has not been achieved yet, the method will be utilized for the OH field measurement in the near future after the developments in laser technology.

The authors greatly appreciate the loan of an imaging spectrograph by Prof. Soji Tsuchiya (Japan Women's University). They would like to thank the referees for reading the manuscript and making a number of helpful suggestions and comments. This work was supported by a Grant-in-Aid for Scientific Research on Priority Areas "Free Radical Science" of the Ministry of Education, Science, Sports, and Culture (Contract No. 05237106).

References

1 P. O. Wennberg, T. F. Hanisco, R. C. Cohen, R. M. Stimpfle, L. B. Lapson, and J. G. Anderson, *J. Atoms. Sci.*, **52**, 3413 (1995).

2 J. R. Barker, "Progress and Problems in Atmospheric Chemistry," World Scientific, Singapore (1995).

3 P. S. Stevens, J. H. Mather, and W. H. Brune, *J. Geophys. Res.*, **99**, 3543 (1994).

4 T. M. Hard, R. J. O'Brien, C. Y. Chan, and A. A. Mehrabzadeh, *Environ. Sci. Technol.*, **18**, 768 (1984).

5 W. Armerding, M. Spiekermann, and F. J. Comes, *J. Geophys. Res.*, **99**, 1225 (1994).

6 M. Hausmann, U. Brandenburger, T. Brauers, and H.-P. Dorn, *J. Geophys. Res.*, **102**, 16011 (1997).

7 F. L. Eisele and D. J. Tanner, *J. Geophys. Res.*, **96**, 9295 (1991); D. J. Tanner and F. L. Eisele, *J. Geophys. Res.*, **100**, 2883 (1995).

8 J. Atmos. Sci., **52**, 3297 (1995).

9 H.-P. Dorn, U. Brandenburger, T. Brauers, M. Hausmann, and D. H. Ehhalt, *Geophys. Res. Lett.*, **23**, 2537 (1996).

10 F. Holland, M. Hessling, and A. Hofzumahaus, *J. Atmos. Sci.*, **52**, 3393 (1995).

11 A. Hofzumahaus, U. Aschmutat, M. Heßling, F. Holland, and D. H. Ehhalt, *Geophys. Res. Lett.*, **23**, 2541 (1996).

12 T. Brauers, U. Aschmutat, U. Brandenburger, H.-P. Dorn, M. Hausmann, M. Heßling, A. Hofzumahaus, F. Holland, C. Plass-Dülmer, and D. H. Ehhalt, *Geophys. Res. Lett.*, **23**, 2545 (1996).

13 G. Zeng, D. E. Heard, M. J. Pilling, and S. H. Robertson, *Geophys. Res. Lett.*, **25**, 4497 (1998).

14 J. D. Bradshaw, M. O. Rodgers, and D. D. Davis, *Appl. Opt.*, **23**, 2134 (1984).

15 L. T. Molina and M. J. Molina, *J. Geophys. Res.*, **91**, 14501 (1986).

16 R. Atkinson, D. L. Baulch, R. A. Cox, R. F. Hampson, Jr., J. A. Kerr, M. J. Rossi, and J. Troe, *J. Phys. Chem. Ref. Data*, **26**, 1329 (1997).

17 W. Armerding, F. J. Comes, and B. Schülke, *J. Phys. Chem.*, **99**, 3137 (1995).

18 K. Shibuya, C. Terauchi, M. Sugawara, K. Aoki, K. Tsuji, and S. Tsuchiya, *J. Mol Struct.*, **413-414**, 501 (1997).

19 A. M. L. Irvine, I. W. M. Smith, R. P. Tuckett, and X.-F. Yang, *J. Chem. Phys.*, **93**, 3177 (1990).

20 J. Luque and D. R. Crosley, *J. Chem. Phys.*, **109**, 439 (1998).

21 R. A. Copeland, J. B. Jeffries, and D. R. Crosley, *Chem. Phys. Lett.*, **138**, 425 (1987).

22 W. L. Dimpfl and J. L. Kinsey, *J. Quant. Spectrosc. Radiat. Transfer*, **21**, 233 (1979).

23 F. H. Mies, *J. Mol. Spectrosc.*, **53**, 150 (1974).

24 G. A. Raiche, J. B. Jeffries, K. J. Rensberger, and D. R. Crosley, *J. Chem. Phys.*, **92**, 7258 (1990).

25 R. A. Copeland, M. J. Dyer, and D. R. Crosley, *J. Chem. Phys.*, **82**, 4022 (1985).

26 D. A. V. Kliner and R. L. Farrow, *J. Chem. Phys.*, **110**, 412 (1999).

27 W. Demtröder, "Laser Spectroscopy," Springer, Berlin (1996).

28 M. de Labachelerie, K. Nakagawa, and M. Ohtsu, *Opt. Lett.*, **19**, 840 (1994).